LOCAL WAVELENGTH ESTIMATION FOR MAGNETIC RESONANCE ELASTOGRAPHY

A. Manduca, R. Muthupillai, P. J. Rossman, J. F. Greenleaf, R. L. Ehman

Depts. of Physiology and Biophysics and Diagnostic Radiology
Mayo Clinic and Foundation
Rochester, MN 55905 USA
E-mail: manduca@mayo.edu

ABSTRACT

A newly developed magnetic resonance imaging technique can directly visualize propagating acoustic strain waves in tissue-like materials [1, 2]. By estimating the local wavelength of the acoustic wave pattern, quantitative values of shear modulus can be calculated and images generated that depict tissue elasticity or stiffness. Since tumors are significantly stiffer than normal tissue (the basis of their detection by palpation), this technique may have potential for "palpation by imaging," with possible application to the detection of tumors in breast, liver, kidney, and prostate. We describe the local wavelength estimation algorithm, study its properties, and show a variety of sample results.

1. INTRODUCTION

A new technique which can directly visualize propagating acoustic strain waves in materials subjected to harmonic mechanical excitation has recently been developed [1, 2]. This technique, termed magnetic resonance elastography (MRE), presents the unique opportunity of generating medical images that depict tissue elasticity or stiffness. This is significant because palpation, a physical examination that assesses the stiffness of tissue, is far more effective at detecting tumors than any current imaging modality, but is restricted to parts of the body that are accessible to the physician's hand. MRE shows promise as a potential technique for "palpation by imaging," with potential applications in the detection of tumors in breast, liver, kidney, and prostate.

The MRE technique incorporates: (i) conventional phase and frequency encoding gradients, (ii) harmonic motion-sensitizing magnetic gradient waveforms, and (iii) synchronous trigger pulses which are fed to a waveform generator driving an electromechanical actuator coupled to the surface of the object being imaged, inducing phase-locked shear waves. MRE images have been acquired which provide snapshots of propagating shear waves (200 - 1100 Hz) in gel phantoms and organ specimens. Wave patterns with displacement amplitudes of less than 200 nanometers are clearly observable. Additionally, these images allow the calculation of regional mechanical properties. In particular, the shear modulus μ of a material is given by $\nu^2\lambda^2\rho$, where ν is the frequency of excitation, ρ the density of the medium, and λ the wavelength of the shear wave in the material. Thus, estimation of the local wavelength (or frequency) of the shear wave propagation pattern at each point in the image allows one to quantitatively calculate local values of shear modulus across the image and generate an image mapping tissue elasticity. These "elastograms" or "stiffness images" clearly depict areas of different elastic moduli in test phantoms, and the calculated values correlate well with moduli calculated independently by mechanical means [1].

2. LOCAL WAVELENGTH ESTIMATION

The classical concept of frequency is not well defined for non-stationary signals, but is so useful that many attempts have been made to define some analogous quantity. The instantaneous frequency, for instance, is commonly defined as the rate of change in phase of the analytic extension of a real signal, though this definition leads to some difficulties and alternatives have been proposed (see Boashash [3, 4] for a review). Many ways to derive local frequency estimates have been proposed, with windowed Fourier transforms and Gabor transforms being the most well-known. Recently, Knutsson et al. [5] described an algorithm which estimates local signal or image frequencies by combining local estimates of instantaneous frequency over a large number of scales, derived from filters which can be considered to be lognormal quadrature wavelets and are a product of radial and directional components.

The filters defined in [5] have a radial component of the form $R_i(\rho) = e^{-C_B \ln^2(\rho/\rho_i)}$ (a Gaussian on a logarithmic scale), where C_B expresses the relative bandwidth and ρ_i is the central frequency. This function is illustrated for six different central frequencies ρ_i in Fig. 1. The directional component has the form $D_k(\hat{u}) = (\hat{u} \cdot \hat{n}_k)^2$ if $(\hat{u} \cdot \hat{n}_k) > 0$ and $D_k(\hat{u}) = 0$ otherwise (where $\hat{n}_k$ is the filter directing vector). This component thus varies as $\cos^2(\phi)$, where ϕ is the angle difference between $\hat{u}$ and the filter direction $\hat{n}_k$, and the filter is non-zero in the positive $\hat{n}_k$ direction only. Along the orientation direction, the filter profiles correspond to the radial component alone, as in Fig. 1.

It is shown in [5] that an isotropic estimate of signal strength, that is local both spatially and in the frequency domain, is obtained by summing the magnitudes of the outputs of orthogonally oriented filters of this kind at one scale, and that the magnitude of the ratio between two lognormal

0-7803-3258-X/96/$5.00

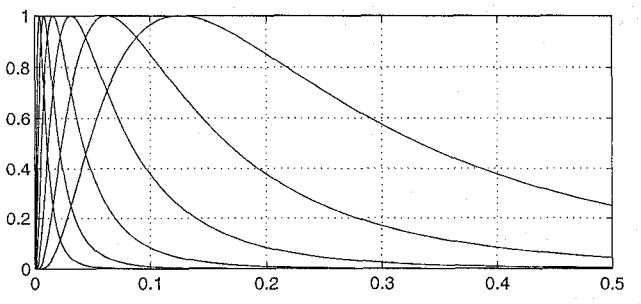

Figure 1: Filter profiles along the orientation direction for six filters with central frequencies spaced an octave apart from 1/256 to 1/8. The bandwidth parameter is $C_B = 1/(2 \ln 2)$.

quadrature filters at different scales can be interpreted as a narrow band estimate of instantaneous frequency. By combining the outputs from two or more sets of filters which differ only in center frequency ρ_i, it is possible to produce a local frequency estimate. If the filters have the appropriate bandwidth relative to the ratio of the two central frequencies [5], a particularly simple case results: the ratio of the two responses times the geometric mean of the two central frequencies is the local frequency estimate. This estimate will work well only if the signal spectrum falls within the range of the filters, but a wide range estimate can be obtained by using a bank of filters and performing a weighted summation over the different filter pairs, with the weighting factor correponding to the amount of energy encountered by each filter pair.

3. RESULTS ON TEST DATA

We have applied this algorithm to test images and to MRE data using (unless otherwise noted) a bank of 6 filter sets, with each set containing both x and y axis oriented filters. Knutsson et al. [5] recommend spacing the central frequencies of such a filter bank an octave apart, which is both a natural choice and one which works well in practice. All our images were 256 x 256 (though some of the figures below are truncated to save space), and we spaced the central filter frequencies an octave apart from 1/256 to 1/8, as shown in Fig. 1. Fig. 2 illustrates that the local frequency estimate is, indeed, isotropic. Fig. 3 shows the results of the algorithm on two test images. The results are displayed using a full gray scale, but the quantitative values in each region correctly match the frequencies used to generate the data set. Vertical profiles across the local frequency estimate images are shown in Fig. 4. The transition region is fairly sharp, and the transition between the two estimates is essentially complete one half wavelength into each region. This results in a sharper transition in the image with shorter wavelengths, as is evident in Figs. 3d and 4; the algorithm is able to utilize the sets of filters at widely different scales to effectively select the appropriate scale for analysis.

To test the effects of noise on the local frequency estimates, we added simple zero-mean Gaussian noise with a standard devation of 10 to the test data in Fig. 3a (whose

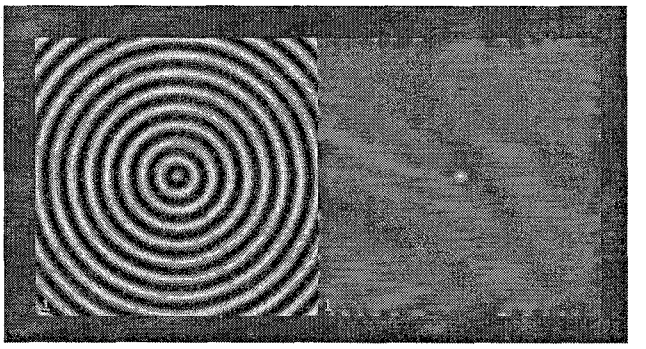

Figure 2: (Left) A test image of a bullseye pattern, in which the profile out from the center in any direction is a sinusoid. (Right) The local frequency estimate image, showing that the estimate is isotropic. The correct value of frequency is recovered everywhere in the image except at the edges (due to wraparound effects) and at the very center (where the local image pattern is not a simple sinusoid).

original values ranged from 0 to 255). The noisy image and the results of the algorithm are shown in Fig. 5, and a vertical profile is shown in Fig 6. The original algorithm now yields estimates that in general are slightly higher than the previous values of 4.0 and 8.0, due to the high frequencies in the noise influencing the averages. Furthermore, these estimates themselves are fairly noisy (see solid line in fig. 6). There is no "correct" answer in this situation, since the underlying signal is not purely a single frequency. However, in practice we would consider it desirable if the algorithm was minimally influenced by such noise and continued to give smooth estimates close to 4.0 and 8.0. This can be accomplished by modifying the algorithm slightly, to use 11 filter sets spaced half an octave apart (and with a reduced bandwith of $C_B = 1/\ln 2$) rather than the default 6 filter sets spaced an octave apart. This modified filter bank clearly gives more accurate, smoother estimates in Figs. 5c and 6 (dashed line).

The modified filter bank covers essentially the same frequency range, with the central frequencies still ranging from 1/256 to 1/8, but the larger number of more precise estimators allow it to estimate a better average frequency at any point. Conversely, viewed in the spatial domain, each of the new fiters has a larger spatial extent (since it has a smaller frequency bandwith), so the new filters are sampling more of space and therefore obtaining better averages over the noise. This implies, however, that the resolution of the modified filter bank should not be as sharp, since the filters are sampling larger spatial regions Looking back at figs. 4a and 4b, we see that this is indeed the case; the modified filters do have a slightly larger transition region. However, the difference is surprisingly small, and one can argue that even in the noise-free case the modified filters might be better since they avoid the slight ringing evident for the standard filter bank in fig. 4b. The modified filter bank requires approximately twice as much computation; execution times are typically 15 sec. for the standard filter bank and 27 sec. for the modified filter bank for 256x256 images on an SGI Indigo 2. Most of this time is spent per-

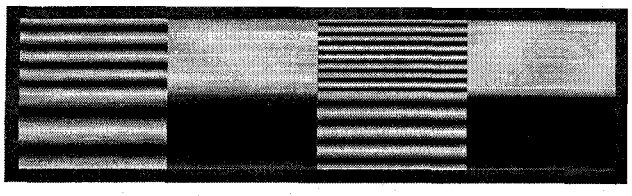

Figure 3: (a) A test image with two regions of different frequencies (4 and 8 cycles/image respectively), (b) the local frequency estimate, (c) a second test image with two regions of higher frequency (8 and 16 cycles/image), and (d) its local frequency estimate. Note how sharply the frequency estimate changes in the transition region; the transition between the two estimates is essentially complete one half wavelength into either region in both cases.

forming FFTs (13 are required for the standard algorithm, 23 for the modified).

4. RESULTS ON MRE DATA

Fig. 7 shows the results of the MRE technique on a gel phantom which contains two cylindrical plugs of different stiffness than the background material. The standard MRI magnitude image (not shown) of this object is simply a uniform field. The mechanical motion is perpendicular to the plane, as is the motion-sensitizing magnetic gradient oscillation. Planar shear waves are generated at the top and propagate down the image. The bright areas in the acoustic strain wave image indicate motion in phase with the magnetic gradient, while the dark areas indicate motion out of phase. The actual displacement values of the motion at any point can be calculated, and correlate well with optical deflection measurements [1, 2]. The wavelength of the shear waves changes as it encounters the plugs of differing stiffness, with the wavelength getting longer in the stiffer plug and shorter in the less stiff plug. Applying the algorithm described above, a local wavelength estimate (LWE) image is obtained, which clearly delineates the two plugs. Fig. 8 shows the results on a phantom with adjacent gel wedges of two different stiffnesses. Refraction effects are clearly visible in the acoustic strain wave image, and in the LWE image the transition between the two regions is sharp and the algorithm's response is clear despite the noise in the data. Finally, Fig. 9 shows the results of imaging an excised porcine kidney. Some distinction is evident between the cortex (outer region) and the medulla (inner region) on the LWE image.

5. CONCLUSION

The Knutsson et al. [5] algorithm appears to be very suitable for local wavelength estimation on MRE data, and for the generation of elasticity images. Since the shear modulus μ of a material is given by $\nu^2\lambda^2\rho$, where ν is the frequency of excitation, ρ the density of the medium, and λ the wavelength of the shear wave in the material, the local wavelength measures at each point can be converted to quantitative measures of shear modulus (a mean density of $1.0g/cm^3$ is an appropriate assumption for tissue-equivalent

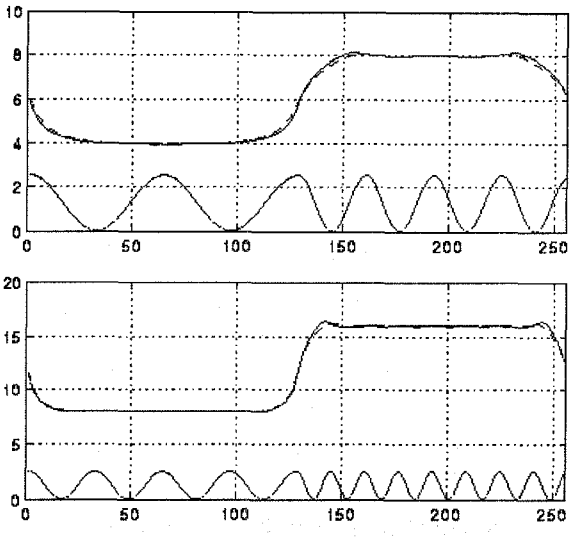

Figure 4: (a) Upper graph: (Top, solid line) A vertical profile along fig. 3b, calculated with the default 6 filter sets. (Top, dashed line) The same profile but calculated with 11 filter sets spaced half an octave apart (see noise suppression discussion below). (Bottom) The vertical profile along fig. 3a, the original data. The left half of the data set (lower half in fig. 3a) has a frequency of 1/64 or 4 cycles across the image, while the right half has a frequency of 1/32 or 8 cycles across the image. (b) Lower graph: (Top, solid line) A vertical profile along fig. 3d, calculated with the default 6 filter sets. (Top, dashed line) The same profile but calculated with 11 filter sets spaced half an octave apart (see noise suppression discussion below). (Bottom) The vertical profile along fig. 3c, the original data. The left half of the data set (lower half in fig. 3c) has a frequency of 1/32 or 8 cycles across the image, while the right half has a frequency of 1/16 or 16 cycles across the image. In both cases, the local frequency estimates yield the correct values in each region and the transition between the two estimates is essentially complete one half wavelength into either region. Note the spatial extent of the transition region is half as large in the lower graph as in the upper graph.

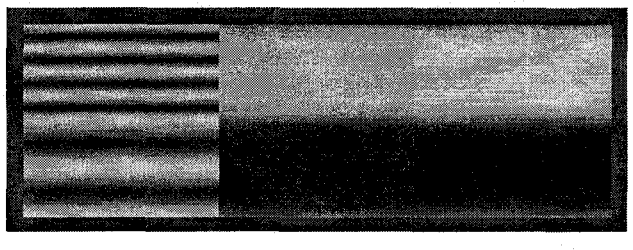

Figure 5: (a) The test image from fig. 3a with Gaussian noise added. (b) The local frequency estimate with the default 6-band filter bank. (c) The local frequency estimate with the 11-band filter bank.

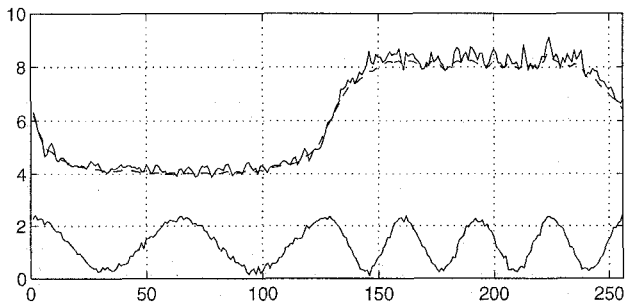

Figure 6: (Top, solid line) A vertical profile along fig. 6b, calculated with the 6-band filter bank. (Top, dashed line) The same profile along fig. 5c, calculated with the 11-band filter bank, with the filters spaced half an octave apart. This estimate is much smoother and closer to the desired values of 4.0 and 8.0. (Bottom) The vertical profile along fig. 5a, the original data.

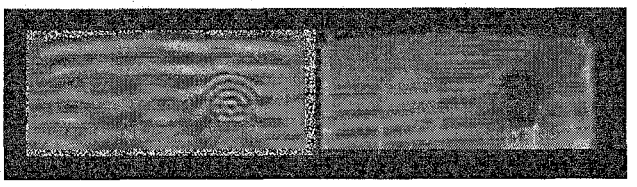

Figure 7: (Left) MRE image of a tissue-simulating gel object containing two embedded gel cylinders with differing stiffness. Shear wave excitation at 250 Hz (perpendicular to the image plane) with an amplitude of 5.0 mm was applied to a wide contact plate on the surface. Planar shear waves are propagating down the image. The cylinder on the left is stiffer than the surrounding gel, resulting in an increased wavelength; conversely, the cylinder on the right is less stiff and shows a shorter wavelength and refraction effects. (Right) The local wavelength estimate of the image. The plugs stand out clearly from the surrounding gel.

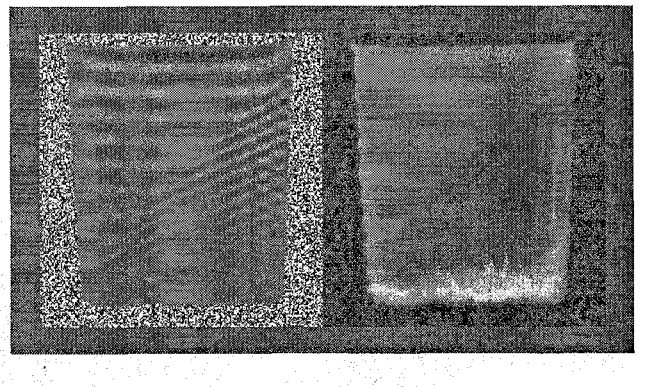

Figure 8: (Left) MRE image of an object with two gel wedges of differing stiffness. Again, planar shear waves are propagating down the image. Refraction effects as the shear waves propagate into the lower (less stiff) gel are clearly visible. (Right) The local wavelength estimate. The transition between the two gels is sharp and the differences in stiffness are clear. Interference effects are visble on the right side of the image, and attenuation effects along the lower edge.

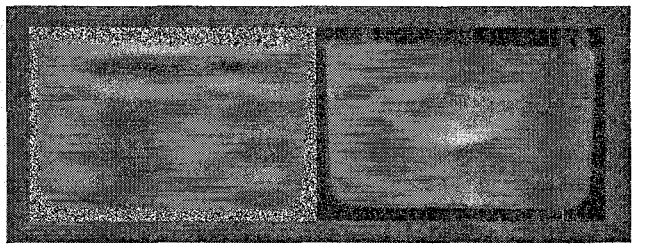

Figure 9: An MRE image of an excised porcine kidney and the local wavelength estimate. The cortex (outer region) of the kidney is stiffer than the medulla (inner region)

gels and soft tissues). The values of shear modulus calculated in test phantoms correlate well with shear moduli calculated independently by other means [1]. Palpation, a physical examination that assesses the stiffness of tissue, has historically been an effective method of detecting tumors, but is restricted to parts of the body that are accessible to the physician's hand. MRE shows promise as a possible technique for "palpation by imaging," with potential applications in the detection of tumors in breast, liver, kidney, and prostate.

6. REFERENCES

[1] Muthupillai R, Lomas DJ, Rossman PJ, Greenleaf JF, Manduca A, Ehman RL, "Magnetic Resonance Elastography by Direct Visualization of Propagating Acoustic Strain Waves," *Science*, 269, pp. 1854-1857, 1995.

[2] Muthupillai R, Rossman PJ, Lomas DJ, Greenleaf JF, Riederer SJ, Ehman RL, "Magnetic Resonance Imaging of Transverse Acoustic Strain Waves," submitted to *Journal of Magnetic Resonance Imaging*, 1996.

[3] Boashash B, "Estimating and Interpreting the Instantaneous Frequency of a Signal - Part 1: Fundamentals," *Proc IEEE*, Vol. 80, pp. 520-538, 1992.

[4] Boashash B, "Estimating and Interpreting the Instantaneous Frequency of a Signal - Part 2: Algorithms and Applications," *Proc IEEE*, Vol. 80, pp. 540-568, 1992.

[5] Knutsson H, Westin CJ, Granlund G, "Local Multiscale Frequency and Bandwidth Estimation," *Proceedings of the IEEE Intl Conf on Image Processing 1994*, Vol. 1, pp. 36-40, 1994.